Pergamon

Int. J. Solids Structures Vol. 32, No. 14, pp. 2063–2075, 1995

0020–7683/95 $9.50 + .00

0020–7683(94)00221–5

FATIGUE CRACK GROWTH IN FIBER–METAL LAMINATES

J. R. YEH
Aluminum Company of America, Alcoa Technical Center, Alcoa Center, PA 15069, U.S.A.

(*Received* 20 *May* 1994; *in revised form* 14 *August* 1994)

Abstract—The fatigue behavior of cracked fiber–metal laminates containing residual stresses is studied. A finite element model employing special interface elements is developed for this study. The use of the interface element allows the simulation to be completed in a single finite element analysis conducted within the limitations of elasticity theory. The effect of crack closure at the crack tip in the aluminum layer is included in the model. Numerical examples are presented for unstretched and stretched ARALL-1 laminates. The results obtained from the finite element model are compared with experimental results. Good agreement between these results supports the validity of the present model.

1. INTRODUCTION

Fiber–metal laminates are stronger and lighter than aircraft alloys used today [see, e.g. Vogelesang *et al.* (1981); Bucci *et al.* (1987); Gunnink and Vogelesang (1991)]. The laminates are made by sandwiching layers of thin aluminum sheet with a fiber-reinforced structural epoxy adhesive. Two types of laminate are available: ARALL™ laminates combine sheets of high-strength aramid fibers with aluminum, and GLARE™ laminates couple glass fibers with aluminum. A schematic representation of the 3/2 ARALL-1 lay-up is shown in Fig. 1. Experimental investigations by Vogelesang *et al.* (1981), and Bucci *et al.* (1987) showed excellent fatigue crack growth properties of ARALL laminates as compared to conventional high-strength aluminum alloys. Moreover, additional fatigue property enhancement of ARALL laminates can be achieved by using a plastic poststraining process [see Bucci *et al.* (1987)]. These comparisons are shown in Fig. 2.

Owing to this great improvement in crack growth properties and high strength-to-weight ratio, the fiber–metal laminates have the potential to be used in weight-sensitive and fatigue-critical structures. In fact, ARALL laminates have been used for the cargo door on the McDonnell Douglas C-17 transport (a military cargo plane). The basic mechanisms of

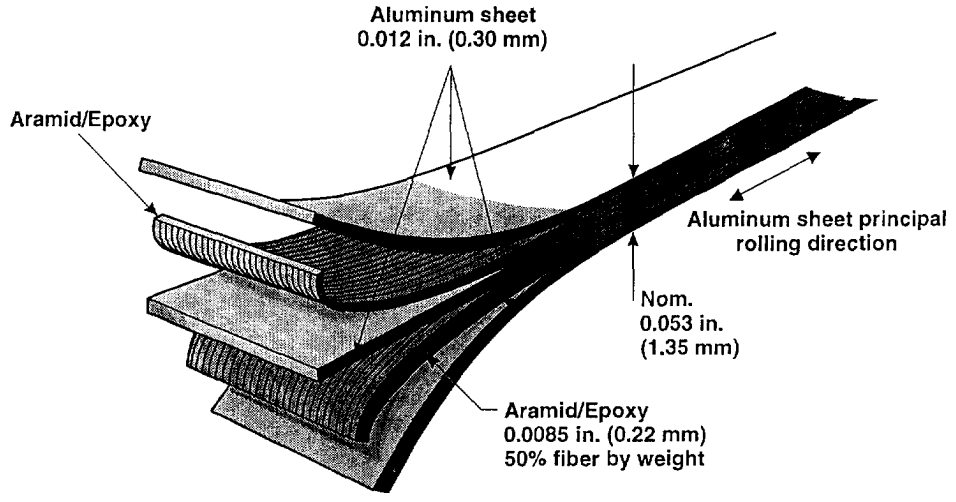

Fig. 1. ARALL laminate standard 3/2 lay-up.

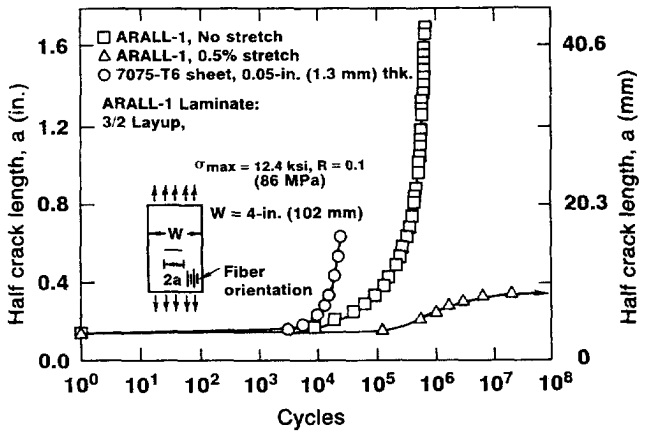

Fig. 2. Fatigue crack growth of stretched and unstretched ARALL-1 laminate and 7075-T6 sheet.

crack growth in fiber–metal laminates are understood and the test results correspond to the qualitative understanding of the material. However, realistic fatigue models are needed for quantitative predictions of the crack growth rate in these laminates. The purpose of this work is to develop a reliable fatigue model, which can be used as a design tool to assist in the selection of fiber–metal laminates for application in fatigue-critical structures.

In this report, a finite element model employing special interface elements is presented and used to quantitatively predict the fatigue crack growth in fiber–metal laminates. In the next section, the basic mechanisms of fiber–metal laminates are discussed. In Section 3, detailed descriptions of the finite element model and the use of the interface element for simulating the crack and delamination advances are given. The technique of using finite element analysis to determine the energy release rates at the crack and delamination tips is addressed in Section 4. The effect of crack closure due to residual stresses is also discussed in Section 4. Finally, several finite element analyses are conducted to demonstrate the applicability of the present model. The finite element results are compared with experimental data whenever possible.

2. FATIGUE MECHANISMS OF FIBER–METAL LAMINATES

The reason for the excellent fatigue properties of fiber-metal laminates is the crack bridging function of the fibers as shown in Fig. 3. When a fatigue crack grows in the aluminum sheets, the fibers stay intact, bridging the crack and thus lowering the energy release rate at the crack tip. The efficiency of the crack bridging mechanism is strongly influenced by the delamination (fatigue debond) at the interface between the aluminum and fiber/epoxy layers (see Fig. 3). Analytical models assuming elliptical delamination between aluminum and fiber/epoxy layers have been developed by Marissen (1984) and Roderick (1978) to study the effects of the crack bridging mechanism. However, the delamination boundary and the crack size are constantly changing during the fatigue loading. Therefore, a system of two coupled mechanisms occurs: (1) crack growth in the aluminum sheets, and (2) delamination growth between the different layers.

Using linear elastic fracture mechanics, the crack growth rate in the aluminum is dependent upon the energy release rate (ΔG_a) at the crack tip according to the Paris' law

$$\frac{da}{dN} = p \cdot \Delta G_a^n \tag{1}$$

where a is the half crack length, N is the number of cycles, and p and n are material constants, which can be determined empirically by crack growth measurements on non-reinforced material.

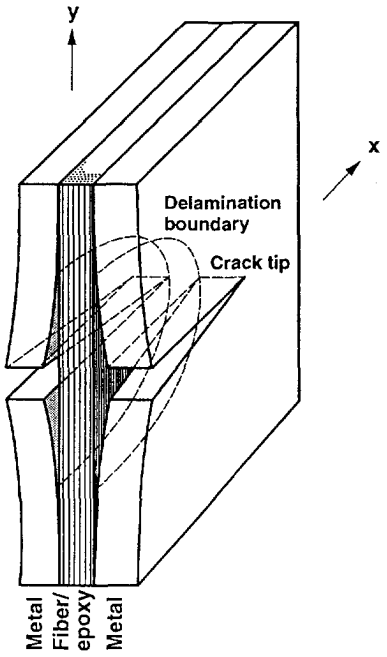

Fig. 3. Schematic of cracked fiber–metal laminate.

Similar to the fatigue crack growth in aluminum, the delamination growth rate may be expressed in terms of the energy release rate ΔG_d along the delamination boundary by the following equation:

$$\frac{dd}{dN} = q \cdot \Delta G_d^m \tag{2}$$

where d is the half delamination length, and q and m are material constants, which can be obtained from delamination growth tests on specimens with a through crack in the aluminum layers [see Marissen (1984) and Awerbuch (1987)]. Note that ΔG_d is assumed constant along the delamination boundary in the models developed by Marissen (1984) and Roderick (1978); however, in the present analysis ΔG_d is allowed to vary along the delamination boundary.

The fatigue behavior of fiber–metal laminates is influenced by the thermal effects as well. As a result of different thermal expansion coefficients for aluminum and fiber/epoxy layers, a tensile residual stress in the aluminum sheets and a corresponding compressive stress in the fiber/epoxy layers will be present due to the hot curing of the laminates. This residual thermal stress system may be reversed by using a plastic poststretching process where the laminate is loaded in such a way that the aluminum is slightly plastically deformed, and the fibers are only deformed elastically. A residual compressive stress in the aluminum sheets and a tensile stress in the fiber layers occur after unloading the laminates. These poststretch residual stresses can cause an additional improvement in the fatigue properties of fiber–metal laminates. As an example, the improvement of an ARALL-1 laminate can be seen in Fig. 2.

In order to simulate the fatigue behavior of cracked fiber–metal laminates, a model must have the following capabilities: (1) to determine the ΔG_a at the crack tip and the ΔG_d along the delamination boundary for the initial thermo-mechanical condition; (2) to calculate the number of cycles needed for crack or delamination tips to grow up to a maximum allowable increment and obtain the new geometries of the crack and delamination using eqns (1) and (2); (3) to determine the ΔG_a at the new location of the crack tip and the ΔG_d along the new location of the delamination boundary; and (4) to repeat (2) and (3), until the crack tip reaches the edge of the aluminum layer. A finite element model that satisfies all the above requirements is described in the next section.

3. FINITE ELEMENT MODEL

In general, the problem of fatigue crack and delamination growth in fiber–metal laminates requires a three-dimensional finite element analysis. In order to solve the problem in two dimensions, several assumptions are made in the finite element model: (1) the geometries of the crack in the aluminum layers and the delamination between the different layers are assumed to be the same throughout the thickness direction; (2) bending flexibilities of the aluminum and fiber/epoxy layers are ignored; (3) aluminum sheet is treated as linearly elastic, since the crack bridging mechanism will considerably reduce the amount of the plastic deformation at the crack tip; (4) the thickness of the aluminum sheet is small compared with the in-plane dimensions, so the plane stress condition is assumed; and (5) in general, the unidirectional fiber/epoxy layer is transversely isotropic and has much stronger elastic properties in the fiber direction than the properties in the transverse direction. In this study, the stiffener direction is parallel to the direction of the fatigue load and perpendicular to the direction of the crack extension. Therefore, the fiber/epoxy layer can be represented by a series of stiffeners attached to the aluminum sheet (see Fig. 4). This assumption is justified by the experimental observation of Marissen (1984) and Teply *et al.* (1987). The stiffeners are assumed to be linearly elastic.

Based on the above assumptions, only one layer of aluminum and one layer of a series of stiffeners are used in the model. A quarter of these two layers is divided into finite elements due to symmetry. Four-node plane stress elements for the aluminum layer and two-node truss elements for the stiffeners are utilized in the finite element model. Higher-order elements are not considered in the analysis because they would greatly complicate the simulation of the crack and delamination extensions. Moreover, the use of these simple elements allows convenient calculation of the energy release rate.

In the finite element model, each stiffener is connected to the aluminum sheet by using a special interface element as shown in Fig. 4. This interface element consists of a series of paired nodes (the nodes have the same x and y coordinates), of which one belongs to the stiffener and the other belongs to the aluminum sheet. The paired nodes are connected by stiff springs in both the x- and the y-directions. As the delamination occurs, the process of debonding is modeled by removing these stiff springs. A similar interface element is also used to model crack growth in the aluminum sheet.

The main advantage of using the interface element is that we can simulate the fatigue behavior of fiber–metal laminates from a single finite element analysis with a number of increments. In each increment, we find the minimum load cycles needed to allow debonding by a node spacing at one interface element. A demonstration of how the model handles the

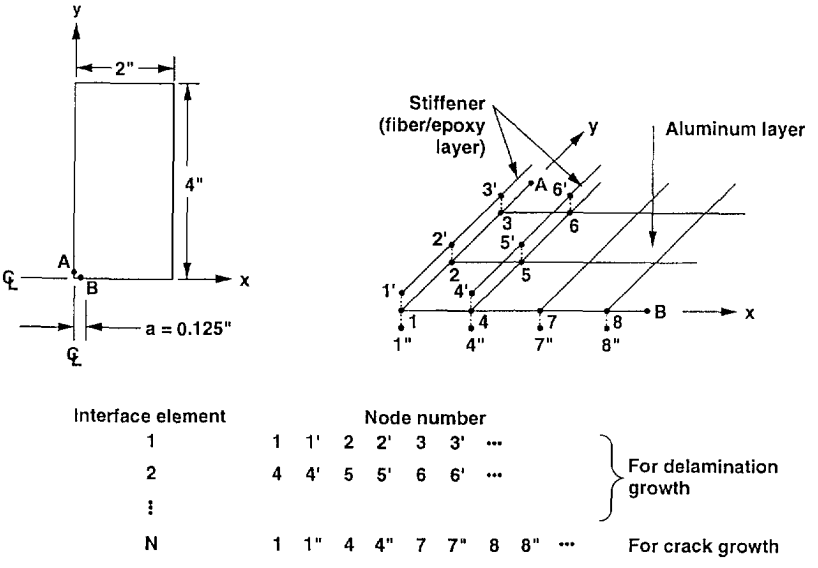

Fig. 4. Geometry and local finite element mesh used in the study.

growth of a crack and delamination is given in the following. Consider a laminate containing a crack as shown in Fig. 5; the location of the crack tip is at node 4. The initial delamination size is assumed to be equal to one node spacing, so the delamination tips are located at nodes 1, 2, and 3. In the first increment, the crack tip is assumed to grow from node 4 to node 5 and the delamination boundary is consequently advanced to a line defined by 1′–2′–3′–6–5. In the second increment, the delamination is assumed to grow from point 1′ to node 7 at a stiffener and the corresponding delamination boundary is defined by the line 7–2″–3″–6′–5′. The number of increments is increased until the crack tip reaches the edge of the aluminum layer. Note that the number of cycles needed for the first increment is obtained by $da/(p \cdot \Delta G_a'')$, in which da is the distance between nodes 4 and 5, and ΔG_a is the energy release rate at the crack tip (node 4). The cycles needed for the following increments are obtained in a similar manner.

The interface element is used not only to model the new debonding length as the crack and delamination advances, but also to calculate the energy release rates, ΔG_a, at the crack tip and ΔG_d at the delamination tip, for each increment. For the calculation of the energy release rate using finite element analysis, the crack and delamination tips need to be located at the nodes of the finite element mesh, and an approximation is made in the model for the crack and delamination tips laying between nodes. The location of these debonding tips are moved back to the nearest node when the ΔG_a and ΔG_d are calculated. For instance, the actual delamination boundary is 1′–2′–3′–6–5 at the beginning of the second increment (see Fig. 5). The boundary 1–2–3–6–5 is used to calculate ΔG_a and ΔG_d. The accuracy of finite element results due to this approximation can be improved by reducing the size of the element. Details of obtaining ΔG_a and ΔG_d for each increment in the finite element analysis are given in the next section.

4. DETERMINATION OF ENERGY RELEASE RATE

An efficient technique of obtaining energy release rates at the crack tip from a coarse finite element mesh was originally introduced by Rybicki and Kanninen (1977) and is extended to the problems of delamination in this study. Detailed discussion of the technique was given by Rybicki and Kanninen (1977). Only relationships relevant to the current problem are given in the following. The technique is based on the crack closure integral introduced by Irwin (1957). Irwin's contention is that if a crack extends by a small amount c, the energy absorbed in the process is equal to the work required to close the crack to its original length [see, e.g. Irwin (1957); Yeh (1989)]. Using a polar coordinate system with the origin at the extended crack tip, the statement in equation form is

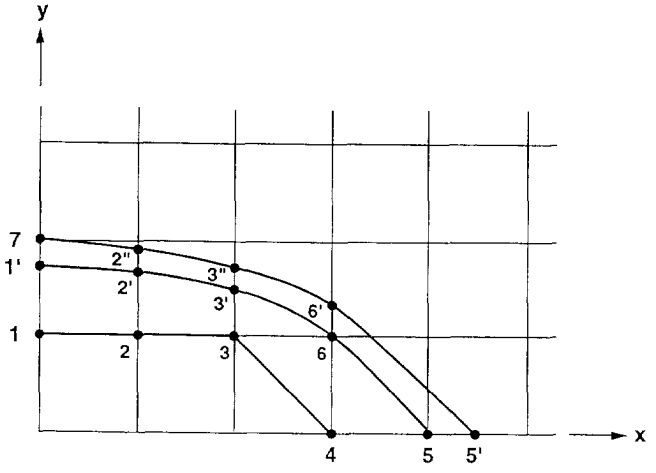

Fig. 5. Schematic of crack and delamination growths.

$$G_{\mathrm{I}} = \lim_{c\to 0} \frac{1}{2c} \int_0^c \sigma_y(r,0) \cdot \bar{v}(c-r,\pi)\, \mathrm{d}r \tag{3a}$$

$$G_{\mathrm{II}} = \lim_{c\to 0} \frac{1}{2c} \int_0^c \tau_{xy}(r,0) \cdot \bar{u}(c-r,\pi)\, \mathrm{d}r \tag{3b}$$

where G_{I} and G_{II} are the energy release rates for modes I and II; σ_y and τ_{xy} are the stresses near the crack tip; and $\bar{u}$ and $\bar{v}$ are the relative sliding and opening displacements between points on the crack faces. To be consistent with the finite element representation (see Fig. 6), eqns (3) can be rewritten in terms of the nodal forces and displacements as follows:

$$G_{\mathrm{I}} = \lim_{c\to 0} \frac{1}{2ct} F_{12} \cdot v_{12} \tag{4a}$$

$$G_{\mathrm{II}} = \lim_{c\to 0} \frac{1}{2ct} T_{12} \cdot u_{12} \tag{4b}$$

where $v_{12} = v_1 - v_2$ and $u_{12} = u_1 - u_2$; t is the thickness of the cracked sheet. The values of F_{12} and T_{12} are taken to be the force normal and parallel, respectively, to the direction of crack advance, that are required to hold nodes 1 and 2 together. In the case when c is much smaller than the crack size, they can be obtained as follows [see Rybicki and Kanninen (1977)]:

$$F_{12} = \left(\frac{c}{h}\right)^s F_{34} \tag{5a}$$

$$T_{12} = \left(\frac{c}{h}\right)^s T_{34} \tag{5b}$$

where h is the length shown in Fig. 6; F_{34} and T_{34} are the forces at the crack tip. These forces are obtained by placing very stiff springs between nodes 3 and 4 and evaluating the forces in the springs. When a crack is embedded in an isotropic medium, the stresses near the crack tip have the $1/\sqrt{r}$ singularity and consequently, s is equal to 0.5 as given by Rybicki and Kanninen (1977). In this section, the energy release rate at the crack tip due to a constant load is discussed. The analysis is more complex when fiber–metal laminates are subjected to cycling loads. Details of obtaining energy release rates at the crack and delamination tips for cycling loads are given in the following sections.

4.1. *Energy release rate at crack tip*

Consider a fiber–metal laminate as shown in Fig. 4. The laminate is subjected to a cyclic constant-amplitude load. The maximum and minimum loads are denoted as $P_{\max}$ and $P_{\min}$, respectively. Due to symmetry, the mode II energy release rate at the crack tip vanishes. The mode I energy release rate (ΔG_{a}) at the crack tip for each increment in the finite element

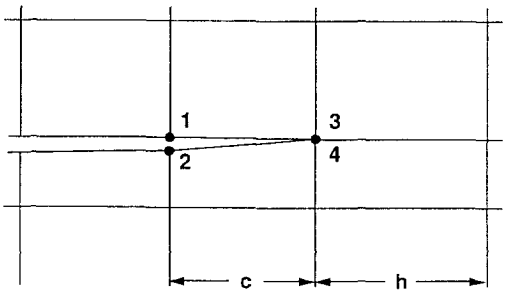

Fig. 6. Finite element nodes near crack tip.

model is determined in two steps. In the first step, we apply the P_{min} to the laminate containing residual stresses and the resulting F_{min} and v_{min} at the crack tip are obtained from the finite element analysis. We substitute P_{min} by P_{max} in the second step and corresponding values for F_{max} and v_{max} are obtained. Then the resulting ΔG_a is given as follows:

$$\Delta G_a = \lim_{c\to 0} \frac{1}{ct_{al}} \int_{v_{min}}^{v_{max}} \left| \frac{(v-v_{min})}{(v_{max}-v_{min})} (F_{max}-F_{min}) + F_{min} \right| dv \tag{6}$$

where t_{al} is the thickness of the aluminum sheet in the finite element model. The above equation is identical to eqn (4a) when P_{min} is assumed to be zero and the laminate is free of residual stress (i.e. $F_{min} = v_{min} = 0$). Note that the accuracy of ΔG_a calculated from the above equation depends upon the number of elements used in the wake of the crack. A sensitivity study is conducted for a center-crack aluminum sheet with the geometry shown in Fig. 4. By comparing the finite element result with the analytical result, it is found that at least five equal-size elements in that region are required for a reliable result.

During the crack propagation, there is an important mechanism, crack closure, which needs to be addressed here, i.e. in some cases, although $P_{max} > P_{min} > 0$, the resulting v_{min} may be smaller than zero due to the influence of the residual stresses in the laminate. In these cases, the lower limit of the integral in eqn (6) should be replaced by zero to include the effect of crack closure. For the case when both v_{min} and v_{max} are smaller than zero, the energy release rate, ΔG_a, is set to zero. In other words, there is no crack propagation at this increment for this cyclic load.

4.2. *Energy release rate at delamination tip*

As pointed out earlier, in the finite element model the fiber/epoxy layer is represented by a series of stiffeners and each stiffener is connected to the aluminum sheet using the interface element. The interface element of each stiffener is capable of modeling the new debonding length as delamination growth, and of determining the energy release rate at the delamination tip. Note that the delamination process in the fiber–metal laminates under in-plane loadings is dominated by the mode II energy release rate (ΔG_d) based on the previous study conducted by the author (Yeh, 1988).

The ΔG_d for each stiffener can be obtained at the same step as the ΔG_a is calculated. For example, we can get T_{min} and u_{min} in the first step and T_{max} and u_{max} in the second step for a stiffener from the same increment of finite element analysis. Then the resulting ΔG_d for the stiffener can be given as follows:

$$\Delta G_d = \lim_{c\to 0} \frac{1}{ct_{st}} \int_{u_{min}}^{u_{max}} \left| \frac{(u-u_{min})}{(u_{max}-u_{min})} (T_{max}-T_{min}) + T_{min} \right| du \tag{7}$$

where t_{st} is the width of the stiffener in the model. The above equation can be reduced to eqn (4b) when P_{min} is assumed to be zero and the laminate is free of residual stresses. Note that the in-plane stresses near the delamination tip are not singular because of the assumption made in the model [the same assumption is used by Marissen (1984)]. Therefore, c is not required to be small compared with the delamination length and s in eqn (5) is set to zero for calculating the force T.

5. NUMERICAL RESULTS AND DISCUSSION

To demonstrate the applicability and accuracy of the finite element model, the ARALL-1 laminate shown in Fig. 1 is studied. The laminate is made of three layers of aluminum sheet and two layers of aramid/epoxy. Material properties of the aluminum and aramid/epoxy are

Table 1. Material properties of aramid/epoxy and aluminum

Aramid/epoxy	
E_{ar}	9098 ksi
α_{ar}	0.8×10^{-6} 1/°C
Aluminum 7075-T6	
E_{al}	10 400 ksi
ν_{al}	0.3
α_{al}	23×10^{-6} 1/°C

listed in Table 1. As discussed earlier, only one layer of aluminum and a series of stiffeners are used in the model. The thickness of the aluminum layer and the stiffeners used in the model are 0.009 in and 0.00425 in, respectively. The material properties, p, n, q, and m, for crack and delamination growth used in the analysis are obtained from experiments conducted by Marissen (1984). They are 1.695×10^{-2}, 1.325, 1.432×10^{10}, and 6.23 for p, n, q, and m, respectively.

The laminate is 4 in wide and 8 in long and is saw-cut (through the thickness) to have a half crack length of $a = 0.125$ in (see Fig. 4). An initial delamination size (d_0) in the wake of the crack needs to be defined in order to include the effect of high interlaminar stresses, which will cause the delamination at the surface of the crack [see Yeh and Tadjbakhsh (1986)]. Three values of d_0 (0.004, 0.008, and 0.012 in) are assumed in the analysis. Residual stress systems in the laminate under the unstretched and stretched conditions are included in the study. The unstretched condition assumes that the laminate is used at room temperature, which is 100°C lower than the curing temperature. The stretched condition assumes that the laminate has a 0.5% residual strain due to a slight plastic deformation of the aluminum after stretch. Since the finite element analysis is conducted within the limits of elasticity, the latter residual stress system is identically reproduced in the study by raising the temperature 207.2°C above the curing temperature, in the aluminum layer.

The finite element results of half crack length *versus* the number of cycles are shown in Fig. 7 for the laminate subjected to a maximum nominal stress, 12.4 ksi, with a stress ratio of $R = 0.1$. It can be seen that in both unstretched and stretched conditions, some variation is observed due to the initial delamination sizes. In general, the smaller the initial delamination length, the larger the number of load cycles required for advancing the crack. For comparison, the experimental results obtained from Bucci *et al.* (1987) are also shown in this figure. Good correlation between the finite element and experimental results is achieved. Note that for the unstretched condition, good agreement is obtained when the initial delamination size (d_0) is given as 0.008 in, which is approximately equal to the thickness of the aramid/epoxy layer (see Fig. 1).

When $d_0 = 0.008$ in, the resulting delamination shape and maximum stress in the stiffeners in the wake of the crack as a function of half-crack length are shown in Figs 8 and 9, respectively, for the unstretched laminate. The results of the stretched laminate are shown in Figs 10 and 11. Although no experimental data are available to verify these results, the resulting delamination shape is very close to the experimental observation by Teply *et al.* (1987) for a stretched ARALL-1 under a similar situation. It can be seen that a very large stress in the aramid/epoxy layer exists at the region near to the saw cut. The amplitude of this large stress reaches its maximum value in the first few increments and then decreases as the crack in the aluminum layer advances. Since the amplitude of this peak stress is smaller than the tensile strength of the aramid/epoxy layer, no fiber failure occurs in the present analysis, which agrees with the experimental observation. Note that the results on the delamination shape and stress distribution in the aramid/epoxy for $d_0 = 0.004$ in and 0.012 in are very close to the results for $d_0 = 0.008$ in, and therefore these results are not given here.

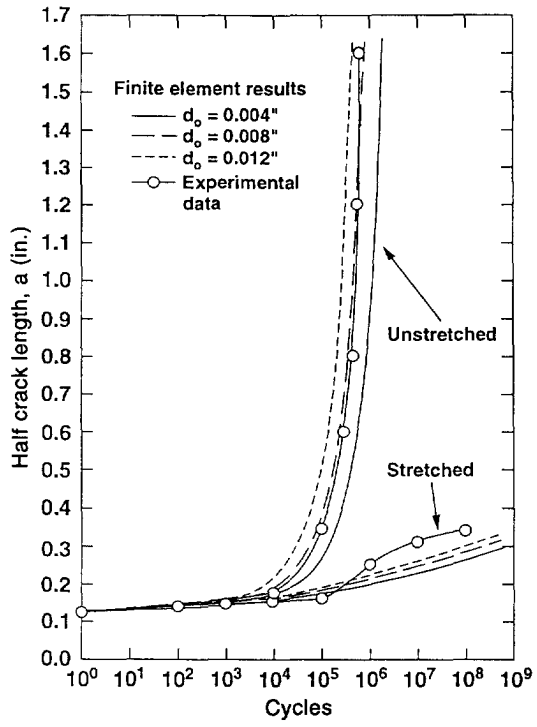

Fig. 7. Comparison of fatigue crack growth of stretched and unstretched ARALL-1 laminate with initial 0.125 in saw cut.

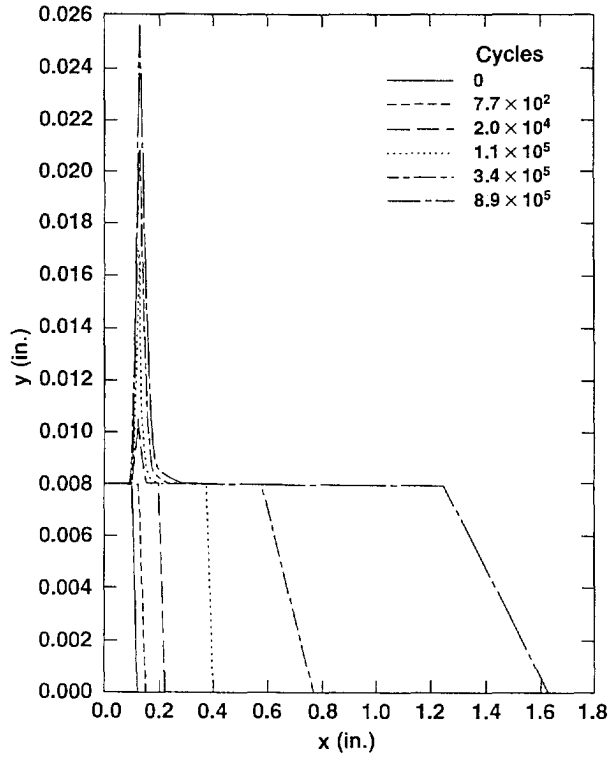

Fig. 8. Fatigue delamination growth in unstretched ARALL-1 laminate with initial 0.125 in saw cut.

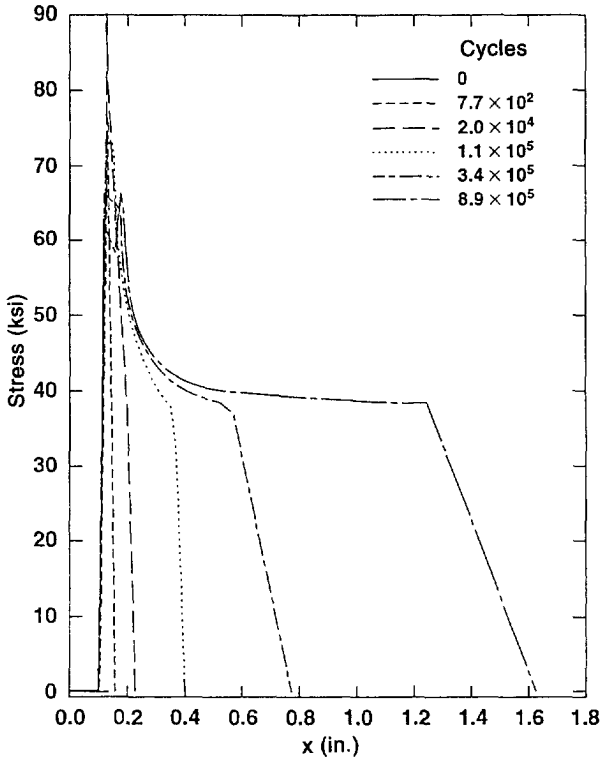

Fig. 9. Maximum stress distribution in aramid/epoxy layer of unstretched ARALL-1 laminate with initial 0.125 in saw cut.

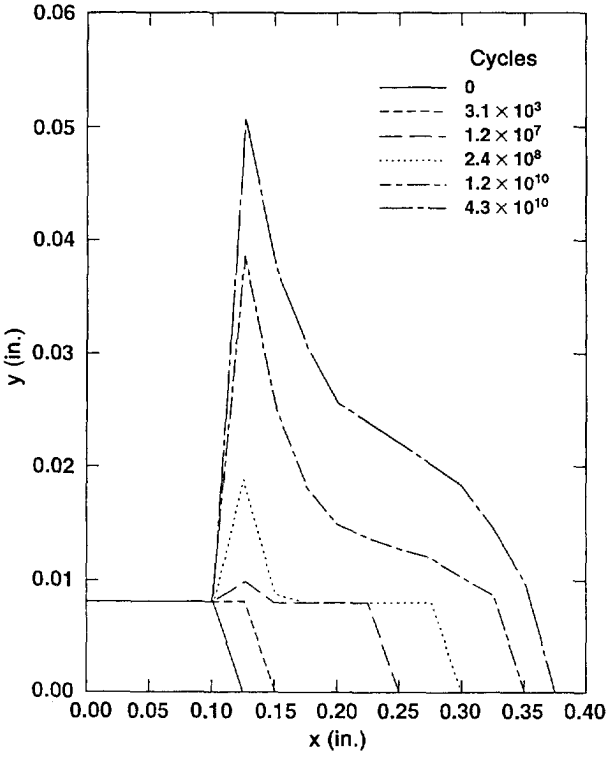

Fig. 10. Fatigue delamination growth in stretched ARALL-1 laminate with initial 0.125 in saw cut.

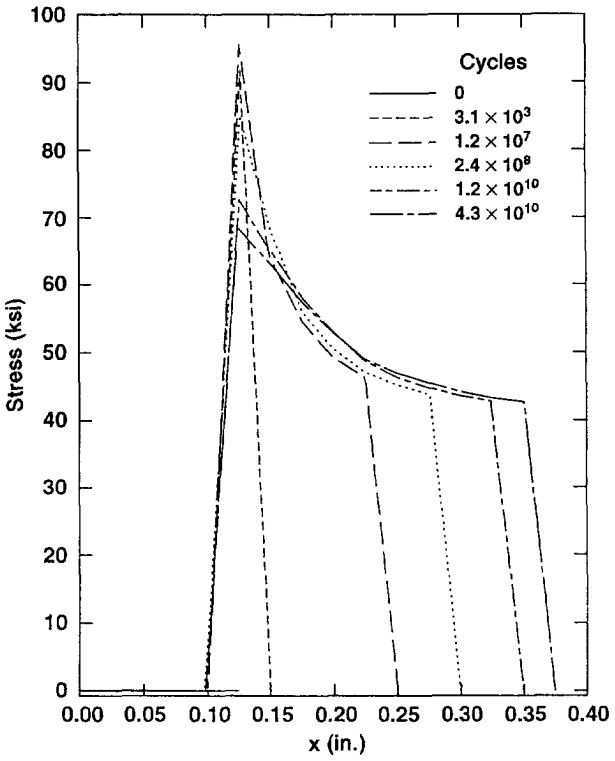

Fig. 11. Maximum stress distribution in aramid/epoxy layer of stretched ARALL-1 laminate with initial 0.125 in saw cut.

In the next example, we assume that the stiffeners in the region of the saw cut are still intact and the initial delamination length equals 0.008 in. The laminate is subjected to a larger maximum nominal stress, 37.2 ksi, with the same stress ratio of $R = 0.1$. The finite element results of half crack length *versus* the number of cycles are shown in Fig. 12 for both unstretched and stretched laminates. As expected, the fatigue life of the stretched laminate is longer than the life of the unstretched laminate.

The resulting delamination shapes as a function of half crack length for the unstretched and stretched laminates are shown in Figs 13 and 14, respectively. It can be seen that the stretched laminate has a limited amount of delamination, while the unstretched laminate has a much larger amount of delamination and the shape of the delamination is very nearly elliptical. The maximum stress in the aramid/epoxy layer in the wake of the crack is almost constant during the delamination process for both laminates. The value of the maximum

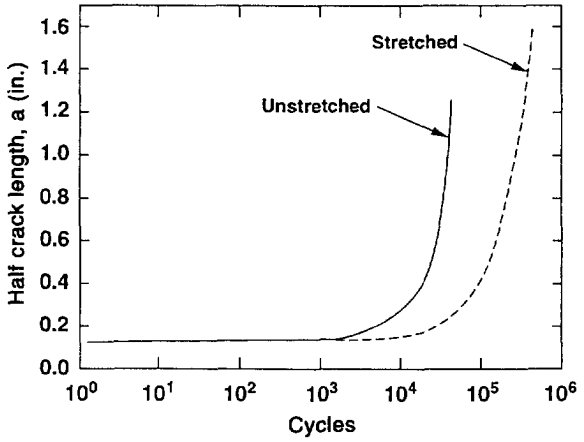

Fig. 12. Fatigue crack growth of stretched and unstretched ARALL-1 laminate with initial 0.125 in crack in aluminum sheet.

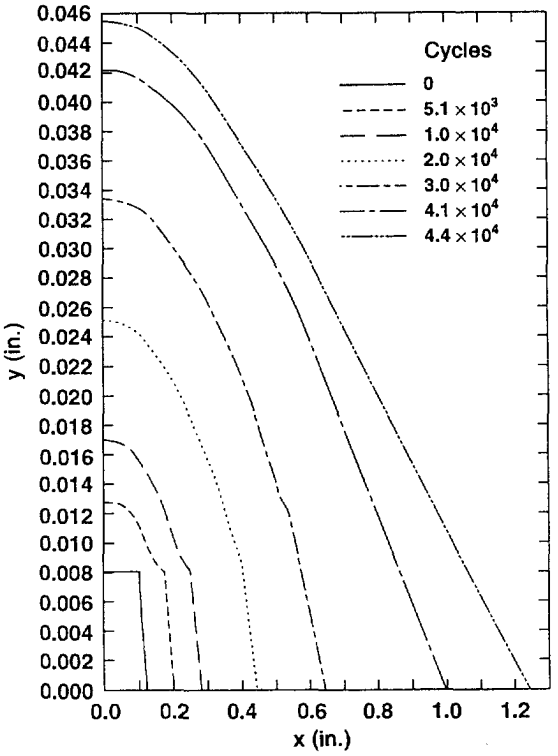

Fig. 13. Fatigue delamination growth of unstretched ARALL-1 laminate with initial 0.125 in crack in aluminum sheet.

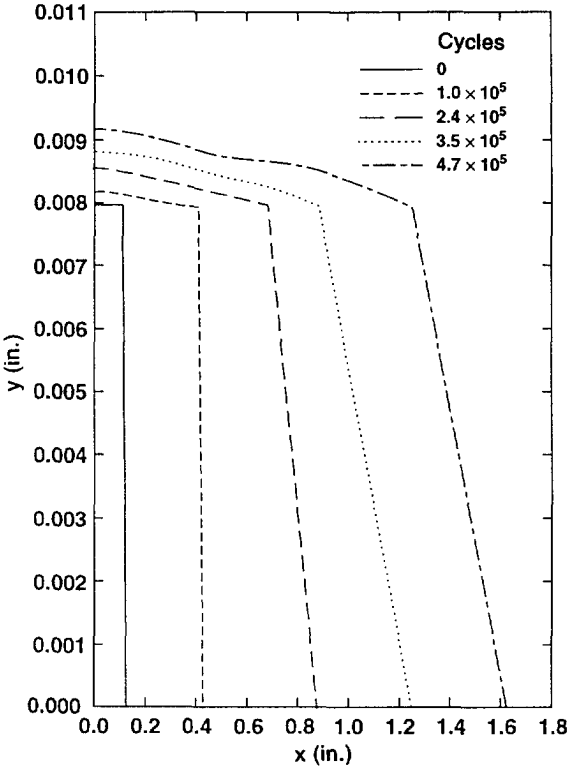

Fig. 14. Fatigue delamination growth of stretched ARALL-1 laminate with initial 0.125 in crack in aluminum sheet.

stress is 110 ksi for the unstretched laminate and 115 ksi for the stretched laminate. These results for the laminate with the intact aramid/epoxy layer support Marissen's model (1984), which assumed that the delamination has an elliptical shape and the stress in the fiber/epoxy layer is a constant in the wake of the crack.

6. CONCLUSIONS

A finite element model employing special interface elements has been developed to study the fatigue behavior of cracked fiber–metal laminates. A system of two coupled mechanisms, crack growth in the aluminum layer and the delamination growth at the interface between the aluminum and aramid/epoxy layers, was analysed using the finite element model. The use of the interface element allows simulation to be completed in a single finite element analysis conducted within the limitations of elasticity theory. The effect of crack closure at the crack tip in the aluminum layer and the residual stresses in the laminate are included in the analysis. The results show that the fatigue life of a stretched laminate is longer than the life of an unstretched laminate.

The present model can be used as a design tool to assist the selection of existing fiber–metal laminates for application in fatigue-critical structures. Also, the model can be used to develop new fiber–metal laminates. For example, the aramid fiber in ARALL and glass fiber in GLARE may be replaced by carbon fiber. It should be mentioned that for any new fiber/epoxy system, the material properties, q and m, of delamination growth need to be obtained from experiments.

Note that the finite element model developed here is for the application of fiber–metal laminates under tension to tension fatigue loads (i.e. $\sigma_{max} > \sigma_{min} > 0$). In the case of laminates subjected to compressive fatigue loads, a local delamination at the interface may lead to buckling problems. The present analysis should not be used in this case, since the effect of buckling is not included in the model.

7. REFERENCES

Awerbuch, J. (1987). Experimental investigation on delamination progression in ARALL laminate. Alcoa Report, Alcoa Technical Center, Pennsylvania.

Bucci, R. J., Mueller, L. N., Schultz, R. W. and Prohaska, J. L. (1987). ARALL laminates—results from a cooperative test program. Paper presented at 32nd International SAMPE Symposium and Exhibition, Anaheim, California.

Gunnink, J. W. and Vogelesang, L. B. (1991). Aerospace ARALL: a challenge for the aircraft designer. In *How Concept Becomes Reality*, pp. 1509–1522. 36th International SAMPE Symposium and Exhibition, San Diego, California.

Irwin, G. R. (1957). Analysis of stresses and strains near the end of a crack traversing a plate. *J. Appl. Mech.* **24,** 361–364.

Marissen, R. (1984). Fatigue crack growth in aramid reinforced aluminum laminates (ARALL)—mechanisms and predictions. DFVLR Institute Fur Werkstoff-Forschnug, Koln.

Roderick, G. L. (1978). Crack propagation in aluminum sheets reinforced with boron-epoxy. PhD Dissertation, Old Dominion University.

Rybicki, E. F. and Kanninen, M. F. (1977). A finite element calculation of stress intensity factors by a modified crack closure integral. *J. Engng Fracture Mech.* **9,** 931–938.

Teply, J. L., DiPaolo, B. A. and Bucci, R. J. (1987). Residual strength of ARALL laminate panels. *19th International SAMPE Technical Conference*, pp. 353–359.

Vogelesang, L. B., Marissen, R. and Schijve, J. (1981). A new fatigue resistant material: aramid reinforced aluminum laminate (ARALL). Paper presented at the ICAF Conference, Noordwijkerhout, The Netherlands.

Yeh, J. R. (1988). Fracture mechanics of delamination in ARALL laminates. *J. Engng Fracture Mech.* **30,** 827–837.

Yeh, J. R. (1989). The mechanics of multiple transverse cracking in composite laminates. *Int. J. Solids Structures* **25,** 1445–1455.

Yeh, J. R. and Tadjbakhsh, I. G. (1986). Stress singularity in composite laminates by finite element method. *J. Composite Mater.* **20,** 347–364.